

# Emergence of Dark Phases in Scalar Particles within the Schwarzschild-Kiselev-Letelier Spacetime

B. V. Simão<sup>1</sup> , M. L. Deglmann<sup>2</sup> , C. C. Barros Jr.<sup>3</sup> .

Departamento de Física, Universidade Federal de Santa Catarina (UFSC), Campus  
Universitário Trindade, Florianópolis, 88035-972, Santa Catarina, Brazil

## Abstract

This work focuses on the emergence of dark phases (dark energy imprints) in the radial wave function of scalar particles. We achieve this by presenting novel solutions of the Klein-Gordon equation in a spherically symmetric spacetime, encompassing a black hole, a quintessential fluid, and a cloud of strings. We determine the exact solution for the spacetime metric, analyze the admissible ranges for its physical parameters, and discuss the event horizon formation. Subsequently, we detail the solution of the Klein-Gordon equation and explore three distinct cases of dark phases, corresponding to the quintessence state parameter  $\alpha_q$  taking the values 0, 1/2, and 1. Notably, the case where  $\alpha_q = 1$  holds particular significance due to current observational constraints on dark energy.

**Keywords:** Dark Energy, Dark Phases, Quintessence, Black Holes, Spin-0 Particles, Heun Equations.

## 1 Introduction

Over the past decades, dark energy-driven cosmology has garnered significant support from multiple independent observations. In addition to groundbreaking data from the luminosity distances of Type Ia supernovae [1, 2], evidence for the universe’s accelerated expansion is corroborated by data from the cosmic microwave background (CMB), baryon acoustic oscillations (BAO), and large-scale structure (LSS) [3, 4]. However, the nature of dark energy remains an open question, with a collective effort underway to determine the equation of state for this cosmic component [5].

In the  $\Lambda$ CDM cosmology, the cosmological constant ( $\Lambda$ ) acts as the dark component, yet it faces substantial challenges [3] which might be addressed by alternative dark energy models. Furthermore, recent findings from the Dark Energy Survey (DES) [6] and the Dark Energy Spectroscopic Instrument (DESI) [7, 8] suggest a dynamical nature for dark energy, thus favoring alternative time-evolving models over the cosmological constant. The class of modified matter models is well represented by the original quintessence model from Caldwell, Dave, and Steinhardt [9] and subsequent developments in scalar field quintessence [3, 4].

In contrast to the works following [9], Kiselev [10] proposed an alternative approach, also termed “quintessence”, where it is understood as an anisotropic, time-independent fluid with positive energy density and negative pressures. This approach offers a simpler

---

<sup>1</sup>vallin.bruna@posgrad.ufsc.br

<sup>2</sup>m.l.deglmann@posgrad.ufsc.br

<sup>3</sup>barros.celso@ufsc.br

way to investigate dark energy. Despite the absence of a time-evolving state parameter, Kiselev’s quintessence can describe particular cosmic epochs where temporal variations might be negligible. Therefore, it allows for the study of the physical outcomes of a specific dark energy regime (see, for instance, [11, 12]).

Another subject of interest concerns how quantum systems are affected by space-time structure and whether a physical observable can be proposed for this purpose. Since Parker’s formulation [13], numerous studies have explored various scenarios, for example, investigating scalar bosons and Dirac particles [14, 15, 16, 17, 18, 19, 20, 21, 22, 23, 24, 25, 26]. However, this question remains far from conclusive.

Building upon this framework, our previous works [27, 28] analyzed scalar particle dynamics in an anti-de Sitter (AdS) spacetime containing a black string (BS), an analogue to clouds of strings (CS), and Kiselev’s quintessence fluid. In these investigations, our primary interest was to determine the effect of quintessence on quantum systems (specifically spin-0 particles) within a cylindrically symmetric spacetime. We demonstrated that the quintessence fluid induces a possible quantum observable, which we termed the *dark phase*. These dark phases allow for the distinction of different values of the dark energy state parameter. These findings highlight the significant role that even static quintessential fluids can play at the quantum level. Consequently, we anticipate that further investigation of these dark phases will yield valuable insights into the fundamental nature of dark energy and its quantum implications.

In the present work, we investigate the emergence of dark phases for spin-0 particles within a spherically symmetric spacetime. Specifically, we analyze the Schwarzschild-Kiselev-Letelier spacetime, which encompasses a black hole, the contribution of the Kiselev quintessential fluid [10], and a cloud of strings [29]. Our aim is to solve the Klein-Gordon equation and determine the occurrence of dark phases for three distinct values of the state parameter  $\alpha_q$ :  $\alpha_q = 0, 1/2$ , and  $1$ . These results will allow us to compare the roles of both quintessence and spacetime symmetry in inducing phase shifts, depending on  $N_q$ .

For this purpose, the paper is organized as follows: In section 2, we introduce the exact metric solution for the Schwarzschild-Kiselev-Letelier spacetime, along with its corresponding energy density and pressure. Section 3 provides parameter estimates for the quintessential component, as well as for the cloud parameter and the Schwarzschild radius. The event horizon formation is analyzed in section 4. In the subsequent sections, we focus on the dark phases, describing the solutions of the Klein-Gordon equation in section 5, and presenting the dark phases in section 6. Finally, section 7 contains our concluding remarks and comparisons.

## 2 Einstein equations

In this work, we aim to study the existence of dark phases and their relevance concerning the other components of the metric. To achieve this, we assume a system composed of a central mass, a cloud of strings, and a Kiselev quintessence fluid. Therefore, in this section, we will determine the metric and the components of the energy-momentum tensor that lead to the desired formulation.

Let us consider the following interval

$$ds^2 = f(r) c^2 dt^2 - \frac{dr^2}{f(r)} - r^2 d\theta^2 - r^2 \sin^2 \theta d\varphi^2, \quad (2.1)$$

associated with the ansatz of a spherically symmetric spacetime, with a *mostly minus* metric signature, related to a Schwarzschild black hole. We take the general Einstein tensor to be

$$G_{\mu\nu} = R_{\mu\nu} - \frac{1}{2}g_{\mu\nu}R, \quad (2.2)$$

where  $R_{\mu\nu}$  is the Ricci tensor and  $R$  is the Ricci scalar. Then, for the metric tensor associated with eq. (2.1), the spherical components  $G_{\mu}^{\nu}$  of the Einstein tensor are

$$G_t^t = G_r^r = \frac{1}{r} \frac{df(r)}{dr} + \frac{f(r)}{r^2} - \frac{1}{r^2}, \quad (2.3)$$

$$G_{\theta}^{\theta} = G_{\varphi}^{\varphi} = \frac{1}{2} \frac{d^2f(r)}{dr^2} + \frac{1}{r} \frac{df(r)}{dr}. \quad (2.4)$$

We consider the Einstein equations to be:

$$G_{\mu}^{\nu} = \frac{8\pi G}{c^4} T_{\mu}^{\nu}. \quad (2.5)$$

It is also important to note that we have chosen to work in the SI units convention to facilitate the interpretation of the theory's physical parameters.

Considering the components of the Einstein tensor given by eqs. (2.3) and (2.4), along with the Einstein equations (2.5), we see that any energy-momentum tensor compatible with this ansatz must be diagonal and possess the same symmetry. Its non-trivial components must satisfy:

$$\begin{aligned} T_t^t &= T_r^r, \\ T_{\theta}^{\theta} &= T_{\varphi}^{\varphi}. \end{aligned} \quad (2.6)$$

In other words, the Einstein equations impose a specific symmetry requirement on the energy-momentum tensor.

In this work, we consider the energy-momentum tensor of quintessence as:

$$\begin{aligned} T_t^t &= T_r^r = \rho_q, \\ T_{\theta}^{\theta} &= T_{\varphi}^{\varphi} = \alpha_q \rho_q. \end{aligned} \quad (2.7)$$

This tensor is compatible with eq. (2.6), and here  $\alpha_q$  is defined by:

$$\alpha_q = -\frac{1}{2}(3\omega_q + 1), \quad (2.8)$$

taking values in the interval  $(0, 1)$  since the standard state parameter  $\omega_q$  satisfies  $\omega_q \in (-1, -1/3)$ .

Additionally, we can incorporate a cloud of strings [29] into this system, whose energy-momentum tensor is given by:

$$\begin{aligned} T_t^t &= T_r^r = \frac{a}{r^2}, \\ T_{\theta}^{\theta} &= T_{\varphi}^{\varphi} = 0, \end{aligned} \quad (2.9)$$

where  $a$  is a real and positive constant ( $a \in \mathbb{R}^+$ ).

With these two sources, the Einstein (2.5) equations become:

$$\frac{1}{r} \frac{df(r)}{dr} + \frac{f(r)}{r^2} - \frac{1}{r^2} = \frac{8\pi G}{c^4} \left( \rho_q + \frac{a}{r^2} \right), \quad (2.10)$$

$$\frac{1}{2} \frac{d^2 f(r)}{dr^2} + \frac{1}{r} \frac{df(r)}{dr} = \frac{8\pi G}{c^4} \alpha_q \rho_q. \quad (2.11)$$

To solve eqs. (2.10) and (2.11), we multiply eq. (2.10) by  $\alpha_q$  and subtract it from eq. (2.11), to show that:

$$r^2 \frac{d^2 f}{dr^2} + 2(1 - \alpha_q) r \frac{df}{dr} - 2\alpha_q f(r) = -2\alpha_q \left( 1 + \frac{8\pi G}{c^4} a \right). \quad (2.12)$$

The associated homogeneous equation is in the form of a Cauchy-Euler equation, implying a solution of the form:

$$f_H = -\frac{r_s}{r} + N_q r^{2\alpha_q}, \quad (2.13)$$

with  $r_s, N_q \in \mathbb{R}^+$ . In addition, the particular solution to eq. (2.12) is simply  $f_P = 1 + 8\pi G a/c^4$  so that the metric function  $f(r)$  is determined by:

$$f(r) = 1 + \bar{a} - \frac{r_s}{r} + N_q r^{2\alpha_q}. \quad (2.14)$$

Here,  $\bar{a}$  is the dimensionless cloud parameter defined by:

$$\bar{a} = \frac{8\pi G}{c^4} a. \quad (2.15)$$

The integration constants  $r_s$  and  $N_q$  are the Schwarzschild radius and the quintessence parameter, respectively.

## 2.1 Quintessence energy density and pressure

Since we have determined  $f(r)$ , given by eq. (2.12), we use the first Einstein equation, (2.10), to obtain the quintessence energy density  $\rho_q(r)$ , which yields:

$$\rho_q(r) = (2\alpha_q + 1) \frac{N_q}{8\pi G/c^4} r^{2\alpha_q - 2}. \quad (2.16)$$

Given that the energy density must be positive, we can see that the condition  $N_q \geq 0$  is compatible with the range of values  $1 < 2\alpha_q + 1 < 3$ . The results for the pressures  $p_\theta = p_\varphi$  follow from eq. (2.7) and are given by

$$p_\theta = p_\varphi = -\frac{\alpha_q (2\alpha_q + 1)}{8\pi G/c^4} N_q r^{2\alpha_q - 2}. \quad (2.17)$$

As expected,  $p_\theta$  and  $p_\varphi$  are indeed negative.

Our next task is to estimate the range of values for these physical parameters to better understand our background spacetime.

### 3 Estimating the physical parameters

To estimate admissible values for the parameters occurring in the metric function  $f(r)$  – namely  $\bar{a}$ ,  $r_s$ , and  $N_q$  – it is useful to consider their dimensions in SI units and relate them with examples from stellar objects. For interested readers, similar approximations were detailed in our previous work [27].

We start by recalling that  $f(r)$  is dimensionless. From this, it immediately follows that the Schwarzschild radius,  $r_s$ , has the dimension of length, i.e.,  $[r_s] = \text{m}$ , in SI units. Typical values for  $r_s$  range from  $10^{-3} \text{ m}$  to  $10^{15} \text{ m}$ .

Furthermore, we emphasize that  $\bar{a}$  is also dimensionless, with admissible values ranging from  $10^{-6}$  to  $10^0$ , analogous to our findings in [27]. The parameter  $a$ , appearing in eq. (2.9), has dimensions of  $[a] = \text{kg m s}^{-2}$  in SI units. This is derived from its definition in eq. (2.15), combined with the dimensions of the fundamental physical constants [30, 31].

Our next step is to estimate the values of  $N_q$ , the quintessence parameter, in terms of the state parameter  $\alpha_q$ . The strategy for this estimation is described in the following subsection.

#### 3.1 The quintessence parameter

To estimate the range of values and the behavior for the quintessence parameter  $N_q$ , we shall first approximate the amount of dark energy in our observable  $\Lambda$ CDM Universe. Let us consider the current radius of the observable Universe as  $r_{\text{obs}}$  and the current dark energy density as  $\rho_{DE}$ , which is assumed to be constant. Based on these simple assumptions, an estimate for the current amount of dark energy (in the observable universe) may be given by:

$$E_{DE} = \frac{4\pi}{3} r_{\text{obs}}^3 \rho_{DE}. \quad (3.1)$$

Now, let us consider the contribution of quintessence and its energy density when the quintessential fluid is the only source of dark energy. To integrate this energy density throughout the whole observable universe, we define:

$$E_q = \int_{V_{\text{obs}}} \rho_q(r) dV = (2\alpha_q + 1) \frac{N_q}{2G/c^4} \int_0^{r_{\text{obs}}} r^{2\alpha_q} dr. \quad (3.2)$$

For this type of estimate, it is sufficient to consider  $dV = r^2 \sin \theta dr d\theta d\varphi$ , in accordance with eq. (2.1). The above definition yields:

$$E_q = \frac{N_q}{2G/c^4} r_{\text{obs}}^{2\alpha_q+1}, \quad (3.3)$$

which is an approximation of the energy contribution from quintessence as a function of  $\alpha_q$  and  $r_{\text{obs}}$ .

Nevertheless, we can require  $E_q = E_{DE}$  to investigate the behavior and orders of magnitude of  $N_q$  for different values of  $\alpha_q$ . By doing so, we obtain that:

$$N_q = \frac{8\pi G}{3c^4} \rho_{DE} r_{\text{obs}}^{2(1-\alpha_q)}, \quad (3.4)$$

where  $\rho_{DE}$  and  $r_{\text{obs}}$  are fixed values. Considering the current radius of the observable Universe to be on the order of  $r_{\text{obs}} \approx 4.4 \times 10^{26}$  m [30, 32] and Dark Energy's energy density to be on the order of  $\rho_{DE} \approx 6 \times 10^{-10}$  J/m<sup>3</sup> [30, 32], we can numerically estimate  $N_q$  as:

$$N_q = \left(4.15 \times 10^{-53}\right) r_{\text{obs}}^{2-2\alpha_q}, \quad (3.5)$$

where we used that  $G/c^4 = 8.24 \times 10^{-45}$  kg<sup>-1</sup> m<sup>-1</sup> s<sup>2</sup> [30]. Given that we are working in SI units, a dimensional analysis shows that  $N_q$  has dimensions of m<sup>-2 $\alpha_q$</sup> .

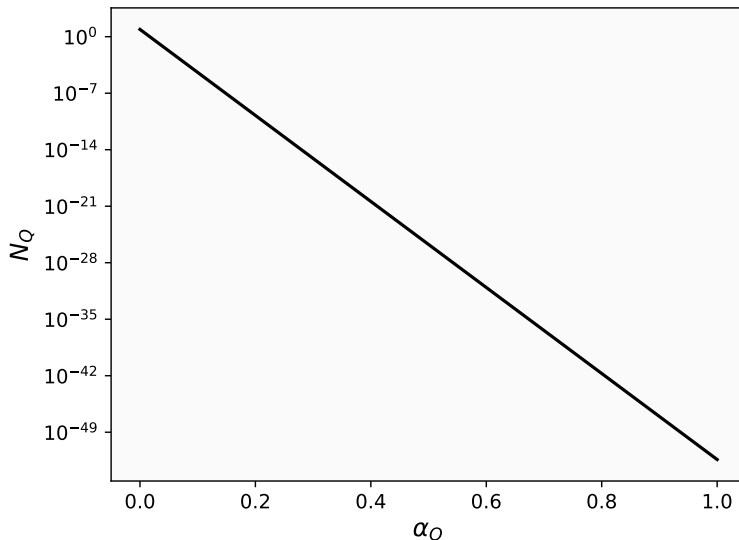


Figure 1: Plot of the quintessence parameter,  $N_q$ , as a function of the state parameter  $\alpha_q$ . As shown in eq. (3.5),  $N_q$  exponentially decreases as  $\alpha_q$  increases.

Finally, we present numerical estimates for  $N_q$  as a function of  $\alpha_q$  in fig. 1. We note that, as  $\alpha_q \rightarrow 1$ , the quintessence parameter  $N_q$  approaches  $4.15 \times 10^{-53}$  m<sup>-2</sup>, in accordance with eq. (3.5).

### 3.2 Contribution to the metric

Now that we have an estimate for the quintessence parameter  $N_q$ , we must investigate the contribution of  $N_q r^{2\alpha_q}$  to the metric function  $f(r)$ . From eq. (3.4), it is straightforward to show that:

$$N_q r^{2\alpha_q} = \frac{2G}{c^4} \frac{E_{DE}}{r_{\text{obs}}} \left(\frac{r}{r_{\text{obs}}}\right)^{2\alpha_q}, \quad (3.6)$$

implying that the contribution from quintessence to the metric becomes significant only when  $r$  is comparable to  $r_{\text{obs}}$ , as long as  $\alpha_q > 0$ . The maximum contribution occurs in the limiting case where  $\alpha_q = 0$ ; as  $\alpha_q$  increases, the quintessence contribution decreases exponentially.

The total amount of dark energy,  $E_{DE} \approx 2.14 \times 10^{71}$  J, was calculated using eq. (3.1) with the values previously specified for  $\rho_{DE}$  and  $r_{\text{obs}}$ . Numerically, eq. (3.6) can be expressed as:

$$N_q r^{2\alpha_q} \approx 8.02 \left(\frac{r}{r_{\text{obs}}}\right)^{2\alpha_q}. \quad (3.7)$$

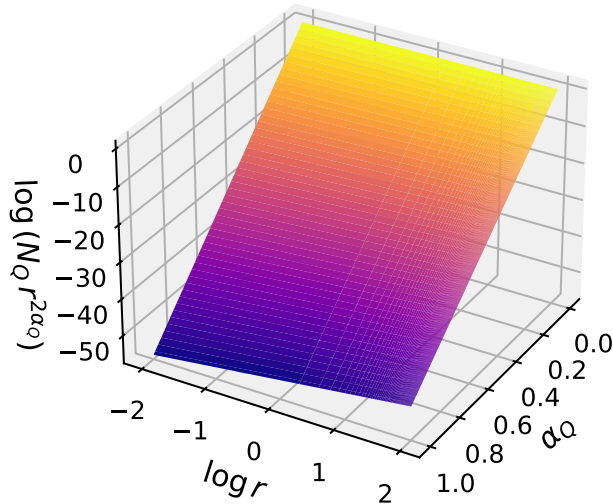


Figure 2: Contribution of the quintessential term on the metric function  $f(r)$ . As represented in eq. (3.7), the influence of the quintessence term is most significant at smaller values of  $\alpha_q$ . In contrast, as the state parameter approaches its upper bound, significantly larger radii are required for the quintessence effect to become substantial.

This is illustrated in fig. 2. As expected,  $N_q r^{2\alpha_q}$  is dimensionless. For completeness, we display in fig. 3 the behavior of the complete metric function for three different values of  $\alpha_q$ , namely  $\alpha_q = 0, 1/2, 1$ . As anticipated, the quintessence parameter is highly sensitive to changes in the state parameter, yielding the most substantial contribution at its lowest value, i.e.,  $\alpha_q = 0$ . Furthermore, while the cloud parameter induces a vertical shift in the metric function, the quintessential term enables horizon formation at considerably smaller distances for the lower bound of  $\alpha_q$  compared to its higher values. In addition, between  $\alpha_q = 1/2, 1$ , the most prominent difference will take place only for  $r \propto r_{\text{obs}}$ , as shown in the inset plot of fig. 3.

#### 4 Event Horizon formation

The existence of event horizons is a fundamental aspect of our analysis. Beyond determining the spacetime structure and, consequently, the behavior of physical particles, the presence of an event horizon provides essential information for solving the Klein-Gordon equation. Therefore, this section investigates this aspect.

Based on the metric function obtained in eq. (2.14), we observe that each value of the state parameter leads to a unique spacetime behavior, resulting in distinct event horizon radii. To address this, we recall that the existence of any event horizon is dependent on the existence of real positive roots of the equation

$$f(r_+) = 1 + \bar{a} - \frac{r_s}{r_+} + N_q r_+^{2\alpha_q} = 0. \quad (4.1)$$

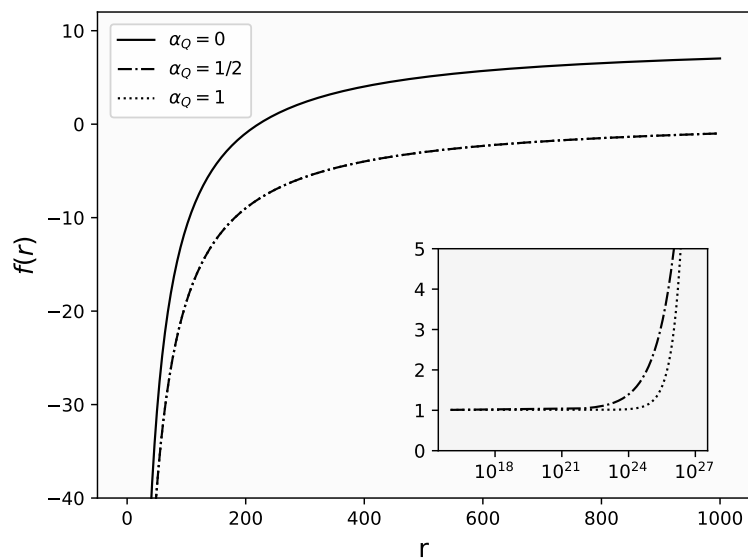


Figure 3: Behavior of the metric function for the state parameter  $\alpha_q = 0, 1/2, 1$ . The cloud contribution and the Schwarzschild radius are set as  $\bar{a} = 10^{-2}$  and  $r_s = 2 \times 10^3$  m, respectively, while the quintessential term is represented according to eq. (3.7), where  $r_{\text{obs}} = 4.4 \times 10^{26}$  m. As highlighted in the inset plot, the curves concerning the two higher state parameters will substantially distinguish themselves near  $r \propto r_{\text{obs}}$ .

Since the state parameter  $\alpha_q$  is continuous, we consider specific values in the interval  $(0, 1)$ , according to which the solutions to eq. (4.1) are classified.

We start with the lower bound of the state parameter ( $\alpha_q = 0$ ), where eq. (4.1) implies that:

$$r_+^{(0)} = \frac{r_s}{1 + \bar{a} + N_q}. \quad (4.2)$$

As it is evident from eq. (4.2), the position of the horizon is directly proportional to the Schwarzschild radius, while  $\bar{a}$  and  $N_q$  equally contribute to regulating  $r_+^{(0)}$ .

On the other hand, when setting  $\alpha_q = 1/2$  in eq. (4.1), one sees that, at the middle of the interval,  $f(r_+)$  satisfies

$$1 + \bar{a} - \frac{r_s}{r_+} + N_q r_+ = 0,$$

which leads to

$$r_+^{(1/2)} = \frac{(1 + \bar{a})}{2N_q} \left[ \sqrt{1 + \frac{4N_q r_s}{(1 + \bar{a})^2}} - 1 \right]. \quad (4.3)$$

When  $N_q r_s / (1 + \bar{a})^2 \ll 1$ , which is a plausible physical regime<sup>4</sup> according to section 3, the event horizon position is well approximated by:

$$r_+^{(1/2)} = \frac{r_s}{(1 + \bar{a})}. \quad (4.4)$$

<sup>4</sup>Remember that, for  $\alpha_q = 1/2$ , the quintessence parameter  $N_q$  is on the order of  $10^{-26} \text{ m}^{-1}$ . Hence, even if we consider  $\bar{a} = 0$  along with  $r_s = 10^{15}$  m, the product  $N_q r_s / (1 + \bar{a})^2 \approx 10^{-11}$ , which readily satisfies the considered regime.

The above result is also the exact solution for when the quintessential fluid is absent, as implied by eq. (4.2). This was expected, because the contribution from the quintessence term is significantly suppressed by the small  $N_q \sim 10^{-26} \text{ m}^{-1}$  (for distances  $r \ll r_{obs.}$ ). As a result, the Schwarzschild radius becomes the dominant factor in horizon formation, which is evident from eq. (4.4). A similar effect is anticipated for the upper bound of the state parameter.

Finally, when  $\alpha_q = 1$ , the condition  $f(r_+) = 0$  implies that:

$$1 + \bar{a} - \frac{r_s}{r_+} + N_q r_+^2 = 0.$$

This equation admits only one real root, given by:

$$r_+^{(1)} = \Delta^{1/3} - \frac{(1 + \bar{a})}{3 N_q} \Delta^{-1/3}, \quad (4.5)$$

with

$$\Delta = \left( \frac{1 + \bar{a}}{3 N_q} \right)^{3/2} \left[ \sqrt{1 + \frac{27}{4} \frac{N_q r_s^2}{(1 + \bar{a})^3}} + \sqrt{\frac{27}{4} \frac{N_q r_s^2}{(1 + \bar{a})^3}} \right].$$

In a previous work on black strings [27], we showed that an equivalent equation for  $r_+^{(1)}$  could be approximated to the form of (4.4) provided that  $N_q r_s^2 / (1 + \bar{a})^3 \ll 1$ . We shall retain this result for future convenience, given that the parameter  $N_q$  is expected to be on the order of  $10^{-52} \text{ m}^{-2}$ . Then, even under the best hypothesis for  $\bar{a}$  and  $r_s$  (to maximize the overall product),  $N_q r_s^2 / (1 + \bar{a})^3$  will be on the order of  $10^{-22}$ .

## 5 The Klein-Gordon equation in the Schwarzschild-Kiselev-Letelier spacetime

Having analyzed the quintessence contribution to the Schwarzschild-Kiselev-Letelier spacetime and its impact on horizon formation, we now turn our attention to the quantum effects that quintessence may exert on the matter content of this background. To address this subject, we investigate the behavior of scalar particles embedded in this spacetime to obtain solutions near the event horizon. These solutions, as will be explored in section 6, exhibit a phase difference due to the quintessence's effect on the spin-0 particle.

For the moment, we proceed with the Klein-Gordon equation in curved spacetime with the mostly-minus sign convention, that is

$$\frac{1}{\sqrt{-g}} \partial_\mu \left( g^{\mu\nu} \sqrt{-g} \partial_\nu \phi \right) + \frac{m_\phi^2 c^2}{\hbar^2} \phi = 0, \quad (5.1)$$

where  $g = \det(g_{\mu\nu})$  and  $m_\phi$  is the spin-0 particle's mass. In addition, the metric tensor  $g_{\mu\nu}$  is fully determined by eq. (2.14).

We decouple eq. (5.1) using the ansatz  $\phi = T(t) R(r) \Theta(\theta) \Phi(\varphi)$ , in which the scalar field  $\phi$  is now expressed with four independent functions, being

$$\phi = e^{-iEt/\hbar} e^{ik\varphi} P_\ell^k(\cos\theta) R(r), \quad (5.2)$$

where  $E$  corresponds to the particle's energy. Moreover,  $k \in \mathbb{Z}$ ,  $\ell \in \mathbb{Z}^+$  and  $P_\ell^k(\cos \theta)$  are Legendre functions, encompassing the angular behavior due to the spherical symmetry. The remaining function  $R(r)$  is the solution to the radial Klein-Gordon equation, given by:

$$R''(r) + \left[ \frac{f'(r)}{f(r)} + \frac{2}{r} \right] R'(r) + \left[ \frac{\epsilon^2}{f(r)^2} - \frac{\bar{m}_\phi^2}{f(r)} - \frac{\ell(\ell+1)}{r^2 f(r)} \right] R(r) = 0, \quad (5.3)$$

where, here, the prime denotes the derivative with respect to  $r$ . The parameters  $\epsilon$  and  $\bar{m}_\phi$  are defined as:

$$\epsilon = \frac{E}{\hbar c}, \quad \text{and} \quad \bar{m}_\phi = \frac{m_\phi c}{\hbar}. \quad (5.4)$$

Therefore, both parameters have units of  $\text{m}^{-1}$  (in SI units).

To handle eq. (5.3) more conveniently, we use the Liouville normal form [33] by introducing an auxiliary function  $u(r)$ , whereas  $R(r)$  is

$$R(r) = \frac{R_0}{r\sqrt{f(r)}} u(r), \quad (5.5)$$

with  $R_0$  being a normalization constant.

In terms of the auxiliary function, the corresponding radial Klein-Gordon equation becomes:

$$u''(r) + V_{\text{eff}}(r) u(r) = 0, \quad (5.6)$$

where  $V_{\text{eff}}(r)$  is identified as the effective potential, satisfying:

$$V_{\text{eff}}(r) = \frac{1}{f(r)^2} \left[ \epsilon^2 + \frac{f'(r)^2}{4} \right] + \frac{1}{f(r)} \left[ -\bar{m}_\phi^2 - \frac{f''(r)}{2} - \frac{f'(r)}{r} - \frac{\ell(\ell+1)}{r^2} \right]. \quad (5.7)$$

At this point, it is convenient to introduce a new coordinate system to explicitly incorporate the event horizon into the radial equation. For this purpose, we adopt the dimensionless coordinate  $x = r/r_+$ . In this new coordinate, the event horizon is located at  $x = 1$ , implying the domain for  $R(x)$  is  $x \in (1, \infty)$ . Accordingly, the effective potential term in the  $x$ -coordinate system becomes:

$$r_+^2 V_{\text{eff}}(x) = \frac{1}{f(x)^2} \left[ r_+^2 \epsilon^2 + \frac{f'(x)^2}{4} \right] - \frac{1}{f(x)} \left[ \frac{1}{2} f''(x) + \frac{f'(x)}{x} + \frac{\ell(\ell+1)}{x^2} + r_+^2 \bar{m}_\phi^2 \right]. \quad (5.8)$$

Therefore, to obtain the radial wave functions near the event horizon (i.e., when  $x \rightarrow 1^+$ ), we consider the first-order approximation of the metric function in the form of

$$f(x) \approx \beta_+(x-1), \quad (5.9)$$

where  $\beta_+$  is defined as  $\beta_+ = r_+[df(r)/dr]|_{r_+}$ . Recalling eq. (2.14), which gives the exact expression of  $f(r)$ , and the constraint  $f(r_+) = 0$ , we determine  $\beta_+$  as:

$$\beta_+ = 1 + \bar{a} + (2\alpha_q + 1) N_q r_+^{2\alpha_q}. \quad (5.10)$$

Note that, substituting eq. (5.9) into eq. (5.8) and performing partial fraction decomposition, the effective potential  $r_+^2 V_{\text{eff}}(x)$  yields:

$$\begin{aligned} r_+^2 V_{\text{eff}}(x) &= \frac{1}{x} \left[ 1 + \frac{\ell(\ell+1)}{\beta_+} \right] + \frac{1}{(x-1)} \left[ -\frac{\bar{m}_\phi^2 r_+^2}{\beta_+} - \frac{\ell(\ell+1)}{\beta_+} - 1 \right] \\ &+ \frac{1}{x^2} \left[ \frac{\ell(\ell+1)}{\beta_+} \right] + \frac{1}{(x-1)^2} \left[ \frac{\epsilon^2 r_+^2}{\beta_+^2} + \frac{1}{4} \right]. \end{aligned} \quad (5.11)$$

Consequently, in the  $x$ -coordinate system, eq. (5.6) exhibits the effective potential given by eq. (5.11), corresponding to the following solution:

$$\begin{aligned} u(x) &= \exp(\alpha x/2) x^{(\beta+1)/2} (x-1)^{(\gamma+1)/2} [c_1 \text{HeunC}(\alpha, \beta, \gamma, \delta, \eta; x) \\ &+ c_2 x^{-\beta} \text{HeunC}(\alpha, -\beta, \gamma, \delta, \eta; x)], \end{aligned} \quad (5.12)$$

where  $\text{HeunC}(\alpha, \pm\beta, \gamma, \delta, \eta; x)$  are confluent Heun functions [34, 35] with the Heun parameters:

$$\begin{aligned} \alpha &= 0, \\ \beta &= \pm 2i \left[ \frac{\ell(\ell+1)}{\beta_+} - \frac{1}{4} \right]^{1/2}, \\ \gamma &= \pm 2i \frac{\epsilon r_+}{\beta_+}, \\ \delta &= -\frac{\bar{m}_\phi^2 r_+^2}{\beta_+}, \\ \eta &= -\frac{1}{2} - \frac{\ell(\ell+1)}{\beta_+}. \end{aligned} \quad (5.13)$$

Using the relation between the radial wave function  $R(x)$  and its auxiliary  $u(x)$ , defined by eq. (5.5), together with the result of eq. (5.12), we conclude that

$$\begin{aligned} R(x) &= (r_+^2 \beta_+)^{1/2} R_0 x^{(\beta-1)/2} (x-1)^{\gamma/2} [c_1 \text{HeunC}(\alpha, \beta, \gamma, \delta, \eta; x) \\ &+ c_2 x^{-\beta} \text{HeunC}(\alpha, -\beta, \gamma, \delta, \eta; x)]. \end{aligned} \quad (5.14)$$

Next, recalling that our solution is valid near the event horizon (positioned at  $x=1$ ), in the regime where eq. (5.9) holds, we investigate the limit of  $R(x)$  as  $x \rightarrow 1^+$ , to conclude that the radial wave function  $R(x)$ , given by eq. (5.14), becomes:

$$R(x) = (x-1)^{\gamma/2} [c_1 x^{\beta/2} + c_2 x^{-\beta/2}], \quad (5.15)$$

where we incorporated  $(r_+^2 \beta_+)^{1/2} R_0$  into the constants  $c_1$  and  $c_2$ . For future convenience in the analysis of dark phases, we rewrite eq. (5.15) as:

$$\begin{aligned} R(x) &= c_1 \exp \left[ \frac{\gamma}{2} \ln(x-1) + \frac{\beta}{2} (x-1) \right] \\ &+ c_2 \exp \left[ \frac{\gamma}{2} \ln(x-1) - \frac{\beta}{2} (x-1) \right], \end{aligned} \quad (5.16)$$

where the Heun parameters  $\gamma$  and  $\beta$  are defined by eq. (5.13). Moreover, we used that  $\ln x \approx (x - 1)$  when  $|x - 1| \approx 0$ . Notably, unless  $|\beta| \gg |\gamma|$ , we see that the dominant term in eq. (5.16) is

$$R(x) \propto (x - 1)^{\gamma/2}, \quad (5.17)$$

so that the real part of the radial wave function is dominated by  $\cos\left[\frac{\gamma}{2} \ln(x - 1)\right]$ . The imaginary part differs by a  $\pi/2$  phase shift. We shall explore this behavior in more detail in the following section.

## 6 Dark Phases

To investigate the quantum implications of dark energy (in the form of Kiselev's quintessential fluid) in scalar particles, we now explore the emergence of quintessence-induced dark phases in the radial wave function  $R(x)$ , determined by eq. (5.16). We continue to explore the scenarios of  $\alpha_q = 0, 1/2, 1$ , along with physical constraints on  $\bar{a}$ ,  $r_s$ , and  $N_q$ . This analysis reveals how quintessence leaves an imprint on scalar particle dynamics, distinguishing the wave functions for different values of the quintessence parameter  $N_q$ . Here, we only consider scenarios where  $r_s \neq 0$ ; otherwise, there would be no event horizon formation.

From eqs. (5.13) and (5.16), we see how the Heun parameters  $\gamma$  and  $\beta$  are fundamental in determining the behavior of the solution shown in eq. (5.16), valid in the vicinity of the event horizon. For this reason, we will have to determine them explicitly for each choice of  $\alpha_q$ . To this aim, it is convenient to use results of eqs. (4.2) and (4.4), together with the general expression of  $\beta_+$ , given by (5.10), to obtain the following results:

$\alpha_q$	$r_+$	$\beta_+$
0	$r_s/(1 + \bar{a} + N_q)$	$1 + \bar{a} + N_q$
1/2	$r_s/(1 + \bar{a})$	$(1 + \bar{a}) [1 + 2 N_q r_s / (1 + \bar{a})^2]$
1	$r_s/(1 + \bar{a})$	$(1 + \bar{a}) [1 + 3 N_q r_s^2 / (1 + \bar{a})^3]$

Table 1: General results of  $r_+$  and  $\beta_+$  for scenarios with  $\alpha_q = 0, 1/2, 1$ . The results in the second row ( $\alpha_q = 1/2$ ) are valid in the physical regime of  $N_q r_s / (1 + \bar{a})^2 \ll 1$ , while those of the third row are valid when  $N_q r_s^2 / (1 + \bar{a})^3 \ll 1$ . Notably, these conditions are easily met when we consider our estimates for  $N_q$ , given by fig. 1.

According to table 1, we can define the following cases, based on the values of  $\bar{a}$ ,  $r_s$ , and  $N_q$ : the standard cases (where all the parameters are non-zero), the cloudless cases (setting  $\bar{a} = 0$ ), and the restricted case without quintessence (setting  $N_q = 0$ ). On the other hand, if we choose a configuration where  $\bar{a} = N_q = 0$ , we fall into the original Schwarzschild case with  $r_+ = r_s$  and  $\beta_+ = 1$ . Notably, our following analysis of dark phases is focused on standard cases, thereby encompassing all relevant contributions.

Having examined the general results for  $r_+$  and  $\beta_+$ , we are able to determine the explicit form of the spin-0 particle's radial wave function near the event horizon for  $\alpha_q = 0, 1/2, 1$ . By doing so, we will discuss the emergence of dark phases, which are similar to our previous results in black string spacetimes [27, 28].

## 6.1 Dark phases at the lower bound

To determine the explicit form of the radial wave function  $R(x)$  for  $\alpha_q = 0$ , we first calculate the Heun parameters  $\gamma$  and  $\beta$ , defined by eq. (5.13). Using the results from table 1, we obtain that:

$$\begin{aligned}\frac{\gamma}{2} &= \pm i \frac{\epsilon r_s}{(1 + \bar{a} + N_q)^2}, \\ \frac{\beta}{2} &= \pm i \left[ \frac{\ell(\ell + 1)}{1 + \bar{a} + N_q} - \frac{1}{4} \right]^{1/2}.\end{aligned}\tag{6.1}$$

Hence, the radial wave function  $R(x)$  can be written as

$$R(x) = c_+ \exp \left[ i \delta_+^{(0)}(x) \right] + c_- \exp \left[ i \delta_-^{(0)}(x) \right],\tag{6.2}$$

where  $\delta_{\pm}^{(0)}(x)$  are given by

$$\delta_{\pm}^{(0)}(x) = \frac{\epsilon r_s}{(1 + \bar{a} + N_q)^2} \ln(x - 1) \pm \left[ \frac{\ell(\ell + 1)}{1 + \bar{a} + N_q} - \frac{1}{4} \right]^{1/2} (x - 1).\tag{6.3}$$

The upper index “ $(0)$ ” associates the functions  $\delta_{\pm}^{(0)}(x)$  to their value of  $\alpha_q = 0$ . Moreover,  $\delta_{\pm}^{(0)}(x)$  encodes the effect of quintessence in the radial wave function  $R(x)$  so that we name it the *dark phase*. Since  $\delta_{\pm}^{(0)}(x)$  are not directly proportional to  $N_q$ , we could use the term *implicit dark phase* to this case. This happens because, from eq. (3.7), we expect  $N_q \approx 8.02$  in the lower bound of  $\alpha_q$ . For such a value of  $N_q$ , we cannot expand the expression to put the quintessence parameter in evidence. A similar result occurred in [28], in the case of a black string spacetime with string clouds and quintessence.

For completeness, we illustrate the effect of  $N_q$  on  $R(x)$  in fig. 4. As  $x \rightarrow 1^+$ , the  $\ln(x - 1)$  term substantially compresses the real part of the non-normalized radial wave function, and this effect becomes even more relevant for small values of  $N_q$ . The impact of the quintessence parameter on the phase is further illustrated in fig. 5. As depicted in the top-left panel, a decrease in  $N_q$  causes  $\delta_+^{(0)}(x)$  to become more pronounced, manifesting as more rapid oscillations in the radial function.

Figure 5 additionally presents the dark phase at the top-right panel as a function of the Schwarzschild radius and the quintessence parameter. Notably, while increasing the order of  $r_s$ , the phase decreases very rapidly as  $N_q$  diminishes. This decay is mitigated as  $N_q$  approaches its expected value. Changes in the cloud parameter, on the other hand, yield minor variations of the phase, as shown in the bottom left panel of fig. 5. This effect is expected when examining the metric function, given by eq. (2.14). At the lower bound, the quintessence term loses its radial dependence and becomes comparable to the cloud parameter. As a result,  $N_q$  becomes dominant over small values of  $\bar{a}$  in eq. (6.3), thereby suppressing the cloud contribution.

Finally, we highlight an interesting feature of eq. (6.3). While panels (a), (b) and (c) in fig. 5 incorporate the choice  $\epsilon = 5 \bar{m}_\phi$  for the spin-0 particle, the bottom right panel depicts the dark phase without imposing a specific mass-dependent energy relation. For higher orders of  $\epsilon$ , the phase becomes progressively intense, implying a decrease in the wavelength as oscillations become faster.

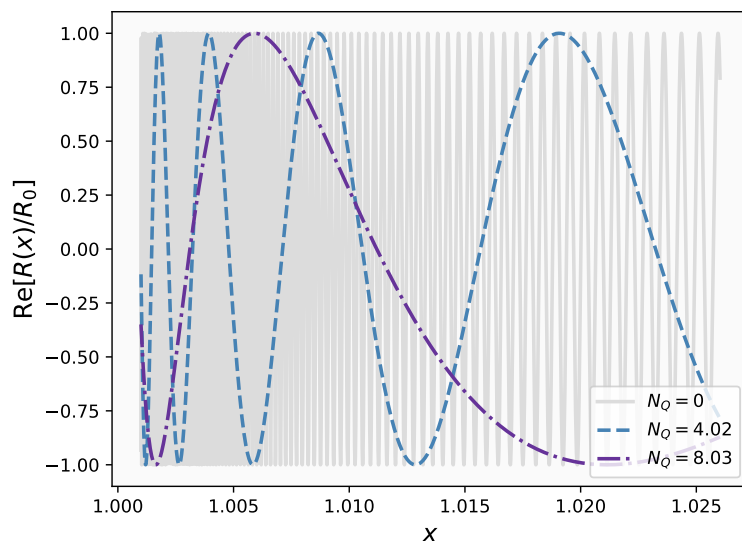


Figure 4: Real part of the non-normalized radial wave function  $R(x)$ , given by eqs. (6.2) and (6.3), as a function of the dimensionless radial coordinate  $x = r/r_+$  for  $\alpha_q = 0$ . The parameters are fixed at  $r_s = 10^2$  m,  $\bar{a} = 10^{-3}$ ,  $\epsilon = 2\bar{m}_\phi$ ,  $l = 3$ , and  $\bar{m}_\phi = 1$  m $^{-1}$  (chosen for visual clarity). For realistic values of  $\bar{m}_\phi = m_\phi c/\hbar$ , the oscillations would be much more rapid, making the distinction between different  $N_q$  values visible only at extremely small distances. Furthermore, note that besides the compression of these oscillations as  $x \rightarrow 1^+$ , due to  $\ln(x-1)$ , the wavelength increases with increasing  $N_q$ .

## 6.2 Dark phases at the middle of the interval

Our next task is to investigate the occurrence of dark phases when  $\alpha_q = 1/2$  (corresponding to  $\omega_q = -2/3$ ). To do so, we use the results from the second row of table 1 to determine the Heun parameters  $\gamma$  and  $\beta$ , given by eq. (5.13), explicitly. This procedure yields:

$$\begin{aligned} \frac{\gamma}{2} &= \pm i \frac{\epsilon r_s}{(1+\bar{a})^2} \left[ 1 - \frac{2N_q r_s}{(1+\bar{a})^2} \right], \\ \frac{\beta}{2} &= \pm i \left[ \frac{\ell(\ell+1)}{1+\bar{a}} - \frac{1}{4} \right]^{1/2} \mp i \frac{\ell(\ell+1)}{(1+\bar{a})} \left[ \frac{\ell(\ell+1)}{1+\bar{a}} - \frac{1}{4} \right]^{-1/2} \frac{N_q r_s}{(1+\bar{a})^2}, \end{aligned} \quad (6.4)$$

where we present a first-order approximation of  $\beta/2$  since  $N_q r_s/(1+\bar{a})^2$  is of the order of  $10^{-11}$  or smaller. Then, substituting the results of eq. (6.4) into the radial wave function of eq. (5.16), we show that  $R(x)$  can be written as

$$R(x) = \Phi_+(x) \exp[-i\delta_+^{(1/2)}(x)] + \Phi_-(x) \exp[-i\delta_-^{(1/2)}(x)], \quad (6.5)$$

where

$$\Phi_\pm(x) = c_\pm \exp \left[ i \frac{\epsilon r_s}{(1+\bar{a})^2} \ln(x-1) \pm i \sqrt{\frac{\ell(\ell+1)}{1+\bar{a}} - \frac{1}{4}} (x-1) \right] \quad (6.6)$$

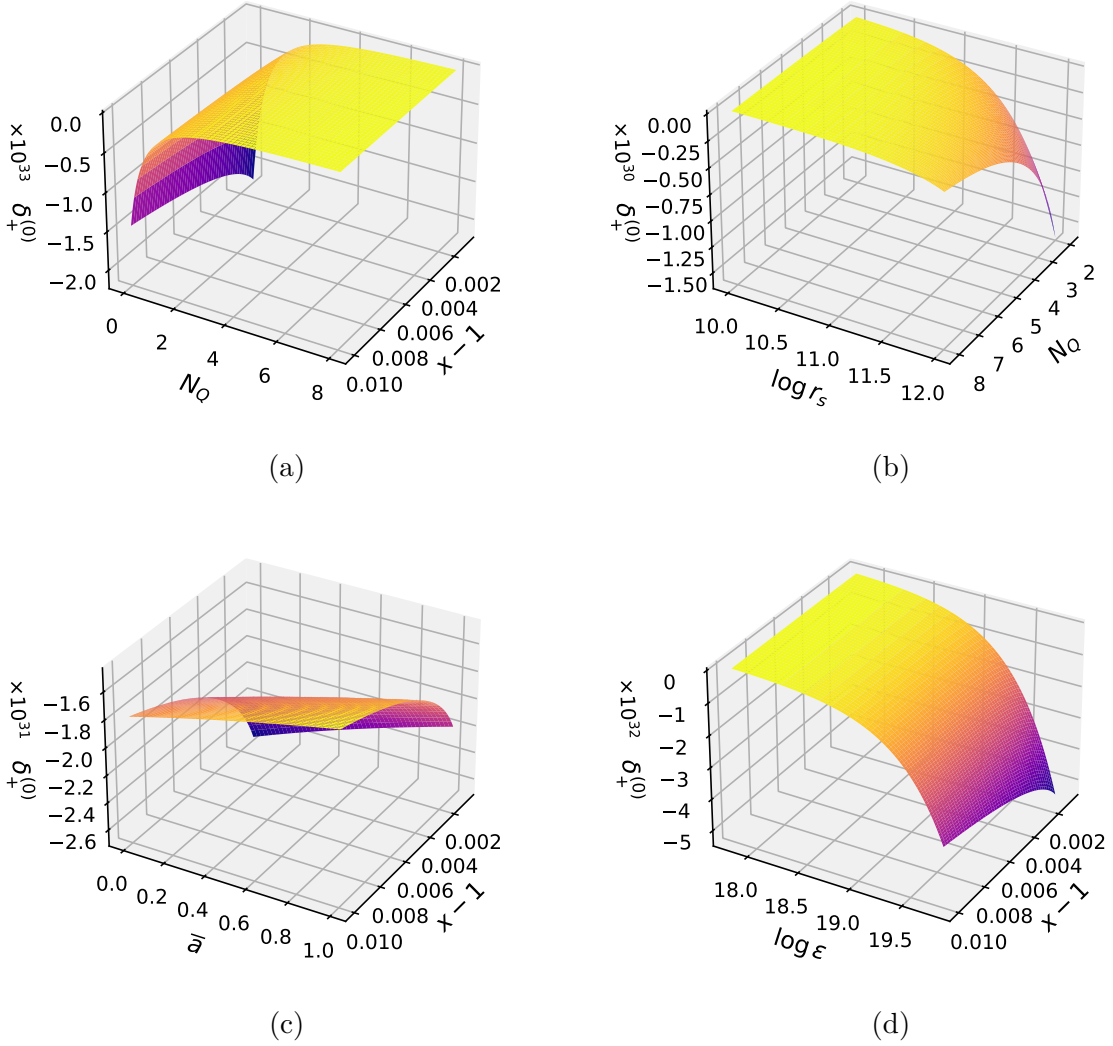


Figure 5: Dark phase at the lower bound, represented by eq. (6.3), as a function of spacetime and particle parameters. For all fixed values, we set  $r_s = 10^{14}$  m,  $\bar{a} = 10^{-3}$ ,  $x = 1.01$  m,  $\ell = 3$  and  $\epsilon = 5 \bar{m}_\phi$ . Furthermore, we considered  $\bar{m}_\phi$  to be the normalized Higgs mass, where  $m_\phi = 2.24 \times 10^{-25}$  kg (see eq. (5.4)), and  $N_q$  is defined according to eq. (3.5) with  $r_{\text{obs}} = 4.4 \times 10^{26}$  m.

is independent of  $N_q$ . The dark phases  $\delta_{\pm}^{(1/2)}(x)$  are determined by:

$$\delta_{\pm}^{(1/2)}(x) = \left[ \frac{2\epsilon r_s}{(1+\bar{a})^2} \ln(x-1) \pm \frac{\ell(\ell+1)}{(1+\bar{a})} \sqrt{\frac{\ell(\ell+1)}{1+\bar{a}} - \frac{1}{4}} (x-1) \right] \frac{N_q r_s}{(1+\bar{a})^2}. \quad (6.7)$$

Therefore, the scalar particle's radial wave function is indeed modified in the presence of our dark energy candidate, and this modification is an explicit phase that increases with  $x$ . We show a numerical example of this case in fig. 6, where the quintessence-induced phase shift is shown for our expected value of  $N_q$ , according to fig. 1, and also for larger values of  $N_q$  (for comparison). However, for  $N_q = 0 \text{ m}^{-1}$  (spacetime without quintessence), the small distances between the peaks of the wave function present numerical challenges, limiting its comparison with  $N_q = 10^{-26} \text{ m}^{-1}$ .

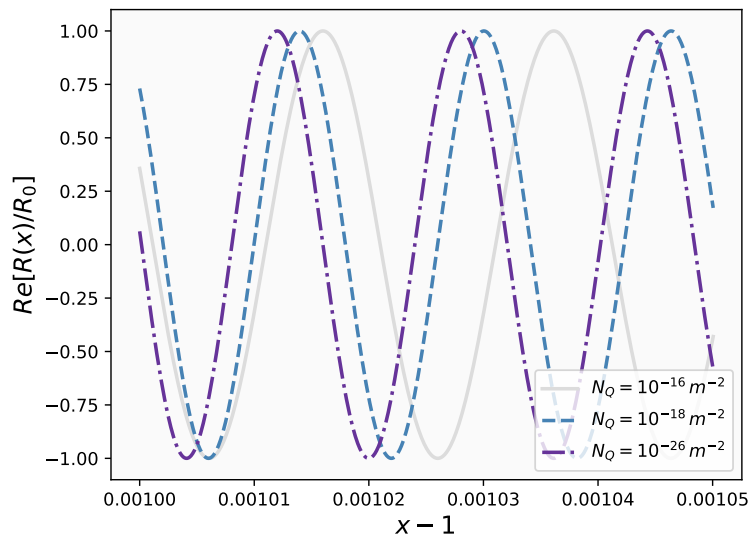


Figure 6: Real part of the non-normalized radial wave function  $R(x)$ , given by eqs. (6.5)–(6.7), as a function of  $x = r/r_+$ , for  $\alpha_q = 1/2$ . The parameters are fixed at  $r_s = 10^{15}$  m,  $\bar{a} = 10^{-6}$ ,  $\epsilon = 4\bar{m}_\phi$ ,  $\bar{m}_\phi = 10^{-13}$  m $^{-1}$  (chosen for visual clarity), and  $l = 3$ . For realistic values of  $\bar{m}_\phi = m_\phi c/\hbar$ , the oscillations would be much more rapid, making the distinction between different  $N_q$  values visible only at extremely small distances. Furthermore, note that the quintessence-induced phase shift increases with  $x$ .

To further analyze the behavior of eq. (6.7), we illustrate in fig. 7 the dark phase as a function of spacetime and particle parameters. As shown in the top-left panel, increasing the quintessence parameter enhances the phase, leading to more rapid oscillations. The Schwarzschild radius also plays a crucial role. Panel (a) employs  $r_s = 10^{14}$  m, whereas the top-right panel displays the phase evolution while for varying  $r_s$  and  $N_q$ . As predicted by eq. (6.7), a larger  $r_s$  yields more intense phases, which can be observed comparing panels (a) and (b).

Within our estimated range for  $\bar{a}$ , we further expect, from eq. (6.7), that increasing the cloud parameter will reduce the compressive effect of the  $\ln(x - 1)$  term on the radial wave function. Concurrently, higher values of the cloud parameter reduce the influence of  $N_q$ . The bottom left panel clearly illustrates this combined effect. Near the horizon, the phase remains reasonably steady for  $\bar{a} < 10^{-2}$ . As  $\bar{a} \rightarrow 1$ , a steep increase in  $\delta_+^{(1/2)}$  occurs, and more intense clouds will exhibit less intense dark phases, thereby producing slower oscillations.

Moreover, the bottom-right panel displays the dark phase as a function of the spin-0 boson’s energy. As  $\epsilon$  increases, the phase becomes notably intense, implying that the real part of the radial function is more compressed at higher energies. This behavior is consistent with that observed in fig. 5 for the lower bound scenario. Nevertheless, fig. 7 reveals that the phase shown in eq. (6.7) is considerably smaller in magnitude when compared to that in eq. (6.3). In fact, the dark phase produced at  $\alpha_q = 1/2$  exhibits an overall moderate phase compared to that at  $\alpha_q = 0$ .

For the lower bound, no expansions were made in the quintessence parameter<sup>5</sup>.

<sup>5</sup>Note that  $N_q \approx 8.02$ .

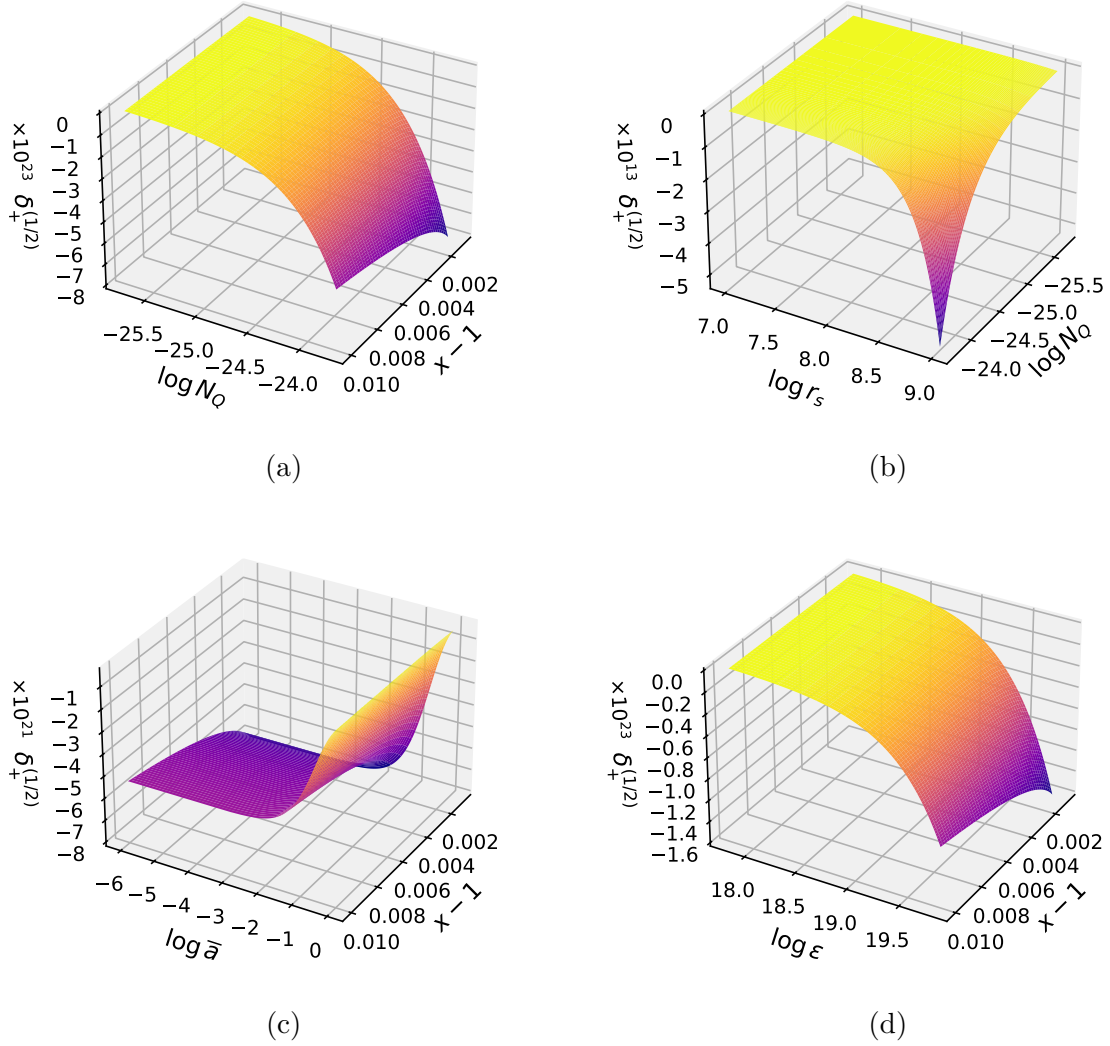


Figure 7: Dark phase at the middle of the interval, given by eq. (6.7), as a function of spacetime and particle parameters. For all fixed values, we set  $r_s = 10^{14}$  m,  $\bar{a} = 10^{-3}$ ,  $x = 1.01$  m,  $\ell = 3$  and  $\epsilon = 5 \bar{m}_\phi$ . Furthermore, we considered  $\bar{m}_\phi$  to be the normalized Higgs mass, where  $m_\phi = 2.24 \times 10^{-25}$  kg (see eq. (5.4)), and  $N_q$  is defined according to eq. (3.5) with  $r_{\text{obs}} = 4.4 \times 10^{26}$  m.

However, at the middle of the interval, the expected value of  $N_q$  is much smaller ( $N_q = 10^{-26} \text{ m}^{-1}$ ), enabling the regime where  $N_q r_s / (1 + \bar{a})^2 \ll 1$ . Within this regime, eq. (6.7) expresses a direct suppression of the  $\ln(x - 1)$  contribution near the horizon, consequently yielding a less intense phase.

Finally, we emphasize that higher-energy spin-0 particles can overcome this suppression, leading to more intense phases. This is evident in the scenario where  $\epsilon$  varies, as depicted in the bottom-right panel of fig. 7. For a specific choice of mass-dependent energy relation, such as  $\epsilon = 5 \bar{m}_\phi$ , this also holds, so that heavier particles yield more intense phases.

### 6.3 Dark phases in the upper bound

Finally, we consider the case of  $\alpha_q = 1$  (or, equivalently,  $\omega_q = -1$ ), where quintessence makes its subtlest contribution to the metric function  $f(r)$ . Nevertheless, this is the most interesting regime, given the current observational constraints on the dark energy equation of state [32, 7, 8].

We begin by determining the explicit Heun parameters  $\gamma$  and  $\beta$  of eq. (5.13). Subsequently, we calculate the final expression for the radial wave function and its resulting dark phase. Using the results from the third row of table 1, in conjunction with eq. (5.13), we show that:

$$\begin{aligned} \frac{\gamma}{2} &= \pm i \frac{\epsilon r_s}{(1+\bar{a})^2} \left[ 1 - \frac{3 N_q r_s^2}{(1+\bar{a})^3} \right], \\ \frac{\beta}{2} &= \pm i \left[ \frac{\ell(\ell+1)}{1+\bar{a}} - \frac{1}{4} \right]^{1/2} \mp i \frac{3}{2} \frac{\ell(\ell+1)}{(1+\bar{a})} \left[ \frac{\ell(\ell+1)}{1+\bar{a}} - \frac{1}{4} \right]^{-1/2} \frac{N_q r_s^2}{(1+\bar{a})^3}. \end{aligned} \quad (6.8)$$

Substituting these expressions for  $\gamma$  and  $\beta$  into the radial wave function given by eq. (5.16), yields:

$$R(x) = \Phi_+(x) \exp \left[ -i \delta_+^{(1)}(x) \right] + \Phi_-(x) \exp \left[ -i \delta_-^{(1)}(x) \right], \quad (6.9)$$

where  $\Phi_{\pm}(x)$  has the exact same expression as eq. (6.6), while the dark phases  $\delta_{\pm}^{(1)}$  are determined by:

$$\delta_{\pm}^{(1)}(x) = \left[ \frac{3 \epsilon r_s}{(1+\bar{a})^2} \ln(x-1) \pm \frac{3}{2} \frac{\ell(\ell+1)}{(1+\bar{a})} \sqrt{\frac{\ell(\ell+1)}{1+\bar{a}} - \frac{1}{4}}^{-1} (x-1) \right] \frac{N_q r_s^2}{(1+\bar{a})^3}. \quad (6.10)$$

As seen from eq. (6.10), these dark phases increase with the distance  $x$ . However, since  $N_q r_s^2 / (1+\bar{a})^3$  is of the order  $10^{-22}$  or smaller, it is challenging to “measure” the induced phase difference between  $N_q = 0 \text{ m}^{-2}$  (when quintessence is absent) and  $N_q = 10^{-52} \text{ m}^{-2}$  (when it is present). For this reason, our numerical example in fig. 8 considers three values for  $N_q$ : the first two representing a Universe supersaturated with dark energy, and the third case being the physically admissible one.

The top-left panel of fig. 9 depicts the dark phase as a function of the quintessence parameter  $N_q$ . Consistent with our previous analysis for  $\alpha_q = 1/2$ , the phase becomes progressively intense as  $N_q$  increases. In addition, the top-right panel illustrates the same behavior upon simultaneous increases in  $N_q$  and  $r_s$ . A key difference, compared to fig. 7, is evident in the order of magnitude of  $\delta_+^{(1)}$ .

Concerning the cloud parameter, we expect the phase to be less intense for larger values of  $\bar{a}$ . This is because larger cloud parameters not only mitigate the effect of the logarithmic term in eq. (6.10), but also minimize the global contribution from  $N_q r_s / (1+\bar{a})^3$ .

Furthermore, fig. 9 illustrates how the dark phase behaves with increasing energy  $\epsilon$  (bottom-right panel). For the case of quintessence at the upper bound ( $\alpha_q = 1$ ), higher-energy spin-0 particles enhance the phase’s magnitude, consistent with the behavior at  $\alpha_q = 0$  and also  $\alpha_q = 1/2$ .

At last, the phases derived for  $\alpha_q = 1$  are considerably smaller in magnitude than those analyzed previously. This is explicitly shown in eq. (6.10), where the term  $N_q r_s^2 / (1+\bar{a})^3 \ll 1$  suppresses the  $\ln(x-1)$  term near the horizon, consequently leading to a less intense phase compared to eq. (6.3) and eq. (6.7).

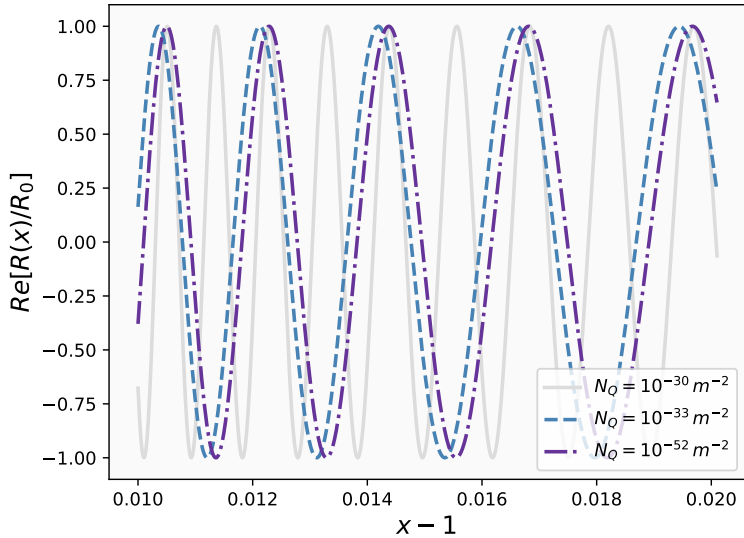


Figure 8: Real part of the non-normalized radial wave function  $R(x)$ , given by eqs. (6.6), (6.9) and (6.10), as a function of  $(x - 1)$ , where  $x = r/r_+$ , for  $\alpha_q = 1$ . The parameters are fixed at  $r_s = 10^{15}$  m,  $\bar{a} = 10^{-6}$ ,  $\epsilon = 4\bar{m}_\phi$ ,  $\bar{m}_\phi = 10^{-12}$  m $^{-1}$ , and  $l = 3$ .

## 7 Conclusions

The emergence of dark phases within the dynamics of scalar particles highlights an interesting aspect of dark energy's influence in the quantum framework. As demonstrated in our previous works [27, 28], these dark phases intrinsically depend on the quintessence parameter  $N_q$ , enabling us to explore the physical consequences of different dark energy state parameters.

Building upon these previous analyses, this work investigated the influence of the quintessence fluid on spin-0 particles. In particular, we considered scalar particles in the vicinity of a Schwarzschild-Kiselev-Letelier black hole horizon, providing detailed solutions to the Klein-Gordon equation for three specific values of the dark energy state parameter ( $\alpha_q = 0, 1/2, 1$ ). To achieve this, we first introduced the exact solution to Einstein's field equations for our specific spacetime and analyzed its effects on event horizon formation. As described in section 4, for  $\alpha_q = 1/2$  and 1, the dark energy parameter becomes significantly small, suppressing the quintessential term in the metric function for distances  $r \ll r_{obs}$ . This effect results in the dominance of the Schwarzschild radius in horizon formation.

Subsequently, by employing a first-order approximation to the metric function, we presented solutions to the Klein-Gordon equation near the event horizon for the aforementioned state parameters. Each of these solutions yielded a unique dark phase, representing the lower, upper, and intermediate bounds of  $\alpha_q$ .

In section 6, we investigated the dependence of the dark phases on the theory's parameters; the results are shown in Figures 4–9. As observed, for some values of these parameters, the dark phases may exhibit more significant effects. A crucial finding from this section was that these dark phases, in spherically symmetric spacetime, are much smaller and subtler than our previous results in cylindrical spacetimes. It appears that, beyond the effect of our dark energy candidate, the geometry of the spacetime itself

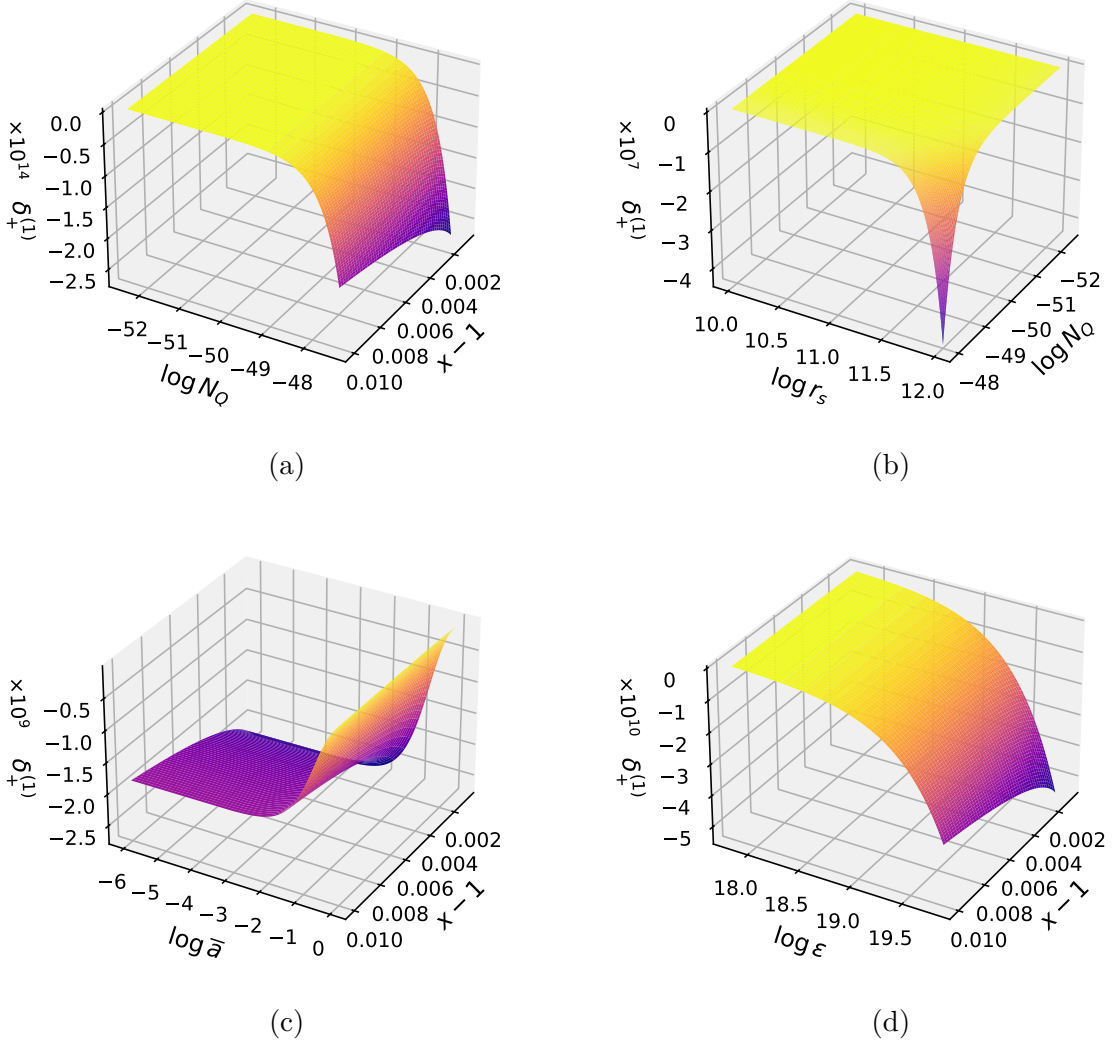


Figure 9: Dark phase at the upper bound, given by eq. (6.10), as a function of spacetime and particle parameters. For all fixed values, we set  $r_s = 10^{14}$  m,  $\bar{a} = 10^{-3}$ ,  $x = 1.01$  m,  $\ell = 3$  and  $\epsilon = 5 \bar{m}_\phi$ . Furthermore, we considered  $\bar{m}_\phi$  to be the normalized Higgs mass, where  $m_\phi = 2.24 \times 10^{-25}$  kg (see eq. (5.4)), and  $N_\phi$  is defined according to eq. (3.5).

influences whether these dark phases are more or less difficult to be “measured”. This novel behavior needs to be investigated further in a subsequent work.

## Acknowledgments

B.V.S. was supported by the Conselho Nacional de Desenvolvimento Científico e Tecnológico (CNPq), grant number 141549/2023-8. M.L.D. would like to thank the Coordenação de Aperfeiçoamento de Pessoal de Nível Superior – Brasil (CAPES) – Finance Code 001. C.C.B.Jr. thanks CNPq, for financial support.

## References

- [1] Adam G. Riess et al. Observational evidence from supernovae for an accelerating universe and a cosmological constant. *Astron. J.*, 116:1009–1038, 1998.
- [2] S. Perlmutter et al. Measurements of  $\Omega$  and  $\Lambda$  from 42 High Redshift Supernovae. *Astrophys. J.*, 517:565–586, 1999.
- [3] Luca Amendola and Shinji Tsujikawa. *Dark Energy: Theory and Observations*. Cambridge University Press, 2010.
- [4] Paul J. Steinhardt. A quintessential introduction to dark energy. *Philosophical Transactions of the Royal Society of London. Series A: Mathematical, Physical and Engineering Sciences*, 361(1812):2497–2513, November 2003.
- [5] Luis A. Escamilla, William Giarè, Eleonora Di Valentino, Rafael C. Nunes, and Sunny Vagnozzi. The state of the dark energy equation of state circa 2023. *JCAP 2405 (2024) 091*, 2024(05):091, May 2023.
- [6] DES Collaboration. Dark energy survey: implications for cosmological expansion models from the final des baryon acoustic oscillation and supernova data. March 2025.
- [7] DESI Collaboration. DESI 2024 VI: Cosmological Constraints from the Measurements of Baryon Acoustic Oscillations. *arXiv e-prints*, page arXiv:2404.03002, April 2024.
- [8] DESI Collaboration. DESI DR2 Results II: Measurements of Baryon Acoustic Oscillations and Cosmological Constraints. *arXiv e-prints*, March 2025.
- [9] R. R. Caldwell, Rahul Dave, and Paul J. Steinhardt. Cosmological imprint of an energy component with general equation of state. *Physical Review Letters*, 80(8):1582–1585, February 1998.
- [10] V V Kiselev. Quintessence and black holes. *Classical and Quantum Gravity*, 20(6):1187–1197, March 2003.
- [11] Ruifang Wang, Fabao Gao, and Huixiang Chen. Particle dynamics around a static spherically symmetric black hole in the presence of quintessence. *Physics of the Dark Universe*, 40:101189, May 2023.
- [12] Javlon Rayimbaev, Uktambek Eshimbetov, Bushra Majeed, Ahmadjon Abdujabbarov, Alisher Abduvokhidov, Bakhrom Abdulazizov, and Akram Xalmirzayev. Test particles and quasiperiodic oscillations around kiselev black hole with cloud of strings\*. *Chinese Physics C*, 48(5):055104, May 2024.
- [13] Leonard Parker. One-Electron Atom in Curved Space-Time. *Phys. Rev. Lett.*, 44(23):1559, 1980.
- [14] Faizuddin Ahmed. The generalized klein–gordon oscillator in the background of cosmic string space-time with a linear potential in the kaluza–klein theory. *The European Physical Journal C*, 80(3), March 2020.

- [15] Emilio Elizalde. Series solutions for the klein-gordon equation in schwarzschild space-time. *Physical review D: Particles and fields*, 36:1269–1272, 09 1987.
- [16] E. O. Pinho and C. C. Barros. Spin-0 bosons near rotating stars. *The European Physical Journal C*, 83(8), August 2023.
- [17] L. C. N. Santos and C. C. Barros. Relativistic quantum motion of spin-0 particles under the influence of noninertial effects in the cosmic string spacetime. *The European Physical Journal C*, 78(1), January 2018.
- [18] L. C. N. Santos and C. C. Barros. Scalar bosons under the influence of noninertial effects in the cosmic string spacetime. *The European Physical Journal C*, 77(3), March 2017.
- [19] L. C. N. Santos, C. E. Mota, and C. C. Barros Jr. Klein–Gordon Oscillator in a Topologically Nontrivial Space-Time. *Adv. High Energy Phys.*, 2019:2729352, 2019.
- [20] A. R. Soares, R. L. L. Vitória, and H. Aounallah. On the Klein–Gordon oscillator in topologically charged Ellis–Bronnikov-type wormhole spacetime. *Eur. Phys. J. Plus*, 136(9):966, 2021.
- [21] R. L. L. Vitória and K. Bakke. On the interaction of the scalar field with a Coulomb-type potential in a spacetime with a screw dislocation and the Aharonov-Bohm effect for bound states. *Eur. Phys. J. Plus*, 133(11):490, 2018.
- [22] R. L. L. Vitória and K. Bakke. Rotating effects on the scalar field in the cosmic string spacetime, in the spacetime with space-like dislocation and in the spacetime with a spiral dislocation. *Eur. Phys. J. C*, 78(3):175, 2018.
- [23] Yi Yang, Zheng-Wen Long, Qi-Kang Ran, Hao Chen, Zi-Long Zhao, and Chao-Yun Long. The generalized Klein–Gordon oscillator with position-dependent mass in a particular Gödel-type space–time. *Int. J. Mod. Phys. A*, 36(03):2150023, 2021.
- [24] Subrahmanyan Chandrasekhar. The solution of dirac’s equation in kerr geometry. *Proceedings of the Royal Society of London. A. Mathematical and Physical Sciences*, 349(1659):571–575, 1976.
- [25] Abdullah Guvendi, Soroush Zare, and Hassan Hassanabadi. Exact solution for a fermion–antifermion system with Cornell type nonminimal coupling in the topological defect-generated spacetime. *Phys. Dark Univ.*, 38:101133, 2022.
- [26] Parisa Sedaghatnia, Hassan Hassanabadi, and Faizuddin Ahmed. Dirac fermions in Som–Raychaudhuri space-time with scalar and vector potential and the energy momentum distributions. *Eur. Phys. J. C*, 79(6):541, 2019.
- [27] M.L. Deglmann, L.G. Barbosa, and C.C. Barros. Black strings and string clouds embedded in anisotropic quintessence: Solutions for scalar particles and implications. *Annals of Physics*, 475:169948, April 2025.
- [28] M. L. Deglmann, B. V. Simão, and C. C. Barros. Extended scalar particle solutions in black string spacetimes with anisotropic quintessence. April 2025.

- [29] Patricio S. Letelier. Clouds of strings in general relativity. *Physical Review D*, 20(6):1294–1302, September 1979.
- [30] S. Navas et al. Review of particle physics. *Phys. Rev. D*, 110(3):030001, 2024.
- [31] Eite Tiesinga, Peter J. Mohr, David B. Newell, and Barry N. Taylor. The 2022 codata recommended values of the fundamental physical constants. Database developed by J. Baker, M. Douma, and S. Kotochigova. Available at <https://physics.nist.gov/constants>, 2024.
- [32] Planck Collaboration. Planck 2013 results. xvi. cosmological parameters. *Astronomy and Astrophysics*, 571:A16, October 2014.
- [33] E.C. Titchmarsh. *Eigenfunction Expansions Associated with Second-order Differential Equations*. Number pt. 1 in Eigenfunction Expansions Associated with Second-order Differential Equations. Clarendon Press, 1962.
- [34] André Ronveaux and Felix Medland Arscott. *Heun's differential equations*. Clarendon Press, 1995.
- [35] F.W.J. Olver, National Institute of Standards, and Technology (U.S.). *NIST Handbook of Mathematical Functions Hardback and CD-ROM*. Cambridge University Press, 2010.